# Electronic structure and lattice dynamical properties of different tetragonal phases of $BiFeO_3$

H. M. Tütüncü* and G. P. Srivastava
*School of Physics, University of Exeter, Stocker Road, Exeter EX4 4QL, United Kingdom*
(Received 18 June 2008; revised manuscript received 5 December 2008; published 31 December 2008)

From first-principles calculations based on the plane-wave pseudopotential method within the density-functional $+U$ scheme, we have investigated the atomic geometry, electronic band-structure, and lattice dynamical properties of four tetragonal phases of the multiferroic $BiFeO_3$. In contrast to the indirect Kohn-Sham band gap of the rhombohedral phase, the most stable of the single-phase stable tetragonal structure is semiconducting with a smaller and direct band gap. It is found that the highest optical phonon branch is split from the rest of the phonon continuum by a small gap. The presently calculated zone-center optical modes have been compared and contrasted with the available polarized Raman-scattering studies and previous calculations based on a simple short-range force-constant method. The highest phonon mode with frequency $\sim 662$ $cm^{-1}$ of $A_1$ representation in the tetragonal phase ($P4mm$) can be readily distinguished from the frequency $\sim 590$ $cm^{-1}$ of $A_2$ representation in the rhombohedral phase ($R3c$).

DOI: 10.1103/PhysRevB.78.235209 PACS number(s): 71.15.Mb, 63.20.dk, 71.20.−b, 77.80.−e

## I. INTRODUCTION

Bismuth ferrite ($BiFeO_3$, henceforth abbreviated as BFO) is currently the subject of extensive research, due to its multielastic multiferroic properties even at room temperature.[1] In its bulk form, BFO assumes the rhombohedral crystal structure. However, free-standing structure of BFO are difficult to grow. Experimentally, BFO thin films are grown by pulsed laser deposition onto single-crystal $SrTiO_3$ (STO) substrates. Highly [111]-oriented rhombohedral BFO films have been grown on STO(111) substrates[2] and [001]-oriented tetragonal BFO films have been grown on STO(001) substrates. A tetragonal phase may only be stabilized by lattice matching the substrate below a critical thickness, depending on the biaxial stress imparted to the film by the substrate during growth. For thicker films, dislocations tend to form and the structure of the film should relax to its bulk geometry. The critical film thickness will also depend on growth conditions. Indeed, there are reports of four different tetragonal phases of BFO films grown on STO(001).[1,3,4]

A large number of investigations have already been carried out on the electronic, electrostatic, and magnetic properties of both these phases of BFO (see, e.g., Wang *et al.*[1]). Zone-center phonon modes of the rhombohedral phase have been studied using the polarized Raman-scattering technique,[2,5,6] using infrared and terahertz techniques,[7] and from lattice dynamical calculations.[2,8,9] A reasonable level of agreement between various studies exists, and a good understanding of the phonon modes has been achieved.

Using the polarized Raman-scattering technique, Singh *et al.*[3] identified several zone-center phonon modes for the tetragonal phase of BFO. These authors also employed a simple short-range force-constant method to calculate all the zone-center phonon modes for this phase. In their theoretical calculations, these authors assumed the key structural parameters of the tetragonal phase as determined previously by Wang *et al.*[1] (in particular, the ratio of the $c$ and $a$ lattice constants was taken as $c/a=1.106$). It has subsequently been found[4] that the key structural parameters of the tetragonal phase of BFO are very sensitive to the laser frequency used during the deposition technique. While the films grown with a 5 Hz laser frequency consist of a mixture of two tetragonal phases (characterized with different values of $a$, $c$, and $c/a$ but both with a small $c/a$ ratio), the films grown with a 15 Hz laser frequency are characterized with a single tetragonal phase (with a different set of values for $a$, $c$, and $c/a$). Ricinschi *et al.*[4] reported on the equilibrium values of the lattice constants ($a$, $c$, and $c/a$), atomic coordinates corresponding to the equilibrium cell dimensions, as well an estimate of the band gap [within the application of the local-density approximation (LDA) of the density-functional theory]. However, it has recently been clearly shown[9] that the electronic band structure and thus the band gap of this material is very sensitive to the scheme adopted for electron-electron interaction. It is, thus, important to undertake a fresh and complete theoretical investigation of the electronic structure and phonon modes for the single-crystal phase of tetragonal BFO.

In this work we have employed an *ab initio* method based on the plane-wave pseudopotential method and the density-functional $+U$ scheme, for calculating the electronic structure of the four different tetragonal phases of BFO[1,3,4] within the $P4mm$ space-group symmetry. Using these results, we extend the calculations within a linear-response scheme to make lattice dynamical calculations. We investigate the energy location and polarization characteristics of the zone-center phonon modes. These results are compared and contrasted with the available polarized Raman-scattering measurements, and a brief discussion is provided on existing disagreements. Essential features of the vibrational density of states (DOS) are also presented.

## II. THEORETICAL DETAILS

Our calculations have been made by using the code PWSCF (Refs. 10 and 11) based on the plane-wave pseudopotential method. The tetragonal symmetry with point-group $4mm$ ($C_{4v}$) and space group $P4mm$ ($C_{4v}^1$) was invoked in all calculations. Ultrasoft pseudopotentials for Bi, Fe, and O were generated by using the VANDERBILT code.[12] As the $3d$ electrons in the transition-metal atom Fe are incompletely

 

filled, the spin-density approximation[13] was employed within the Perdew-Burke-Ernzerhof (PBE) form[14] of the generalized gradient ($\sigma$GGA) scheme. The effect of Coulomb repulsion between the localized Fe $3d$ states was treated by employing a simplified rotational-invariant formulation of the $\sigma$GGA$+U$ method.[15] In this approach an effective on-site interaction parameter is defined as $U_{\text{eff}}=U-J$, where $U$ and $J$ describe the Hubbard on-site Coulomb repulsion and exchange interaction, respectively. An equivalent interpretation of this scheme would be to consider $J=0$ and treat $U_{\text{eff}}=U$. We will adopt the latter interpretation and thus talk about $U$ as the only parameter in this work. Kohn-Sham single-particle wave functions were expanded in a plane-wave basis up to 60 Ry kinetic-energy cutoff. For geometry optimization and electronic band-structure calculations, Brillouin-zone integration was performed by using the $6\times6\times6$ Monkhorst-Pack **k**-points grid.[16] The structures in this work were fully relaxed using force as well as stress minimization schemes. In order to avoid ambiguities regarding the free-energy results, we have always used the same energy cutoff and the same **k**-points grid for convergence in all calculations. A criterion of at least 0.01 meV/atom was placed on the self-consistent convergence of the total energy. Brillouin-zone integration was performed with a Gaussian broadening of 0.015 Ryd during all relaxations.

Using the electronic structure results as input, phonon calculations at the zone center, along crystal symmetry directions, as well as at all the Monkhorst-Pack grid points, were carried out by employing the density-functional linear-response technique as described by Baroni *et al.*[10] As phonon calculations are computationally much more intensive, we first evaluated dynamical matrices on the $4\times4\times4$ Monkhorst-Pack grid. These dynamical matrices were Fourier transformed to obtain the full phonon spectrum and density of states.

## III. RESULTS

### A. Atomic geometry, phase stability, and Fe magnetic moment

For the sake of clarity and ease of discussion, we will label the four tetragonal structures studied here as follows: *structure I* for the sample grown by Wang *et al.*,[1] *structure II* and *structure III* for the coexistant phases I and II, respec-

TABLE I. Atomic geometry, stability, and local magnetic moment at the Fe atom for different tetragonal structures of BFO determined within the $\sigma$GGA scheme. For structures I–III the experimentally reported cell parameters were considered. For structure IV the starting cell parameters were taken as the experimentally reported values and then theoretically optimized. For all structures, internal parameters (i.e., atomic coordinates) were fully optimized. The relaxed atomic geometry is expressed in lattice coordinates. These results are compared with the corresponding values for the rhombohedral bulk structure.

| Tetragonal structures | Structure I (experimental cell parameters[a]) | | | Structure II (experimental cell parameters[b]) | | | Structure III (experimental cell parameters[b]) | | | Structure IV (theoretical cell parameters[b]) | | |
|---|---|---|---|---|---|---|---|---|---|---|---|---|
| $a$ (Å) | 3.935 | | | 3.77 | | | 3.88 | | | 3.67 | | |
| $c$ (Å) | 3.998 | | | 4.65 | | | 4.07 | | | 4.64 | | |
| $c/a$ | 1.016 | | | 1.233 | | | 1.049 | | | 1.264 | | |
| Volume (Å$^3$) | 61.91 | | | 66.09 | | | 61.28 | | | 62.50 | | |
| Atomic geometry | | | | | | | | | | | | |
| Bi | 0.0 | 0.0 | 0.0000 | 0.0 | 0.0 | 0.0000 | 0.0 | 0.0 | 0.0000 | 0.0 | 0.0 | 0.0000 |
| Fe | 0.5 | 0.5 | 0.4147 | 0.5 | 0.5 | 0.4392 | 0.5 | 0.5 | 0.4218 | 0.5 | 0.5 | 0.4525 |
| O | 0.5 | 0.5 | −0.1228 | 0.5 | 0.5 | −0.1704 | 0.5 | 0.5 | −0.1232 | 0.5 | 0.5 | −0.1559 |
| | 0.5 | 0.0 | 0.3385 | 0.5 | 0.0 | 0.2944 | 0.5 | 0.0 | 0.3390 | 0.5 | 0.0 | 0.3037 |
| | 0.0 | 0.5 | 0.3385 | 0.0 | 0.5 | 0.2944 | 0.0 | 0.5 | 0.3390 | 0.0 | 0.5 | 0.3037 |
| Relative energy (eV/cell) | 0.16 | | | −0.18 | | | 0.16 | | | 0.0 | | |
| Fe magnetic moment ($\mu_B$) | 4.18 | | | 4.95 | | | 4.14 | | | 4.90 | | |
| Rhombohedral structure[c] | | | | | | | | | | | | |
| $a$ (Å) | 5.66 | | | | | | | | | | | |
| Volume per BFO unit (Å$^3$) | 60.215 | | | | | | | | | | | |
| Atomic geometry | | | | | | | | | | | | |
| Bi($2a$) | 0.000 | 0.000 | 0.000 | | | | | | | | | |
| Fe($2a$) | 0.221 | 0.221 | 0.221 | | | | | | | | | |
| O(6b) | 0.530 | 0.936 | 0.389 | | | | | | | | | |
| Relative energy (eV/BFO unit) | −0.43 | | | | | | | | | | | |
| Fe magnetic moment ($\mu_B$) | 3.87 | | | | | | | | | | | |

[a]Reference 1.
[b]Reference 4.
[c]Reference 9.

TABLE II. Comparison of structural parameters, local magnetic moment at the Fe atom, and the equatorial oxygen plane vibrational frequency $B_1$ at the zone center for tetragonal BFO (structure IV) from the applications of the LSDA and $\sigma$GGA schemes for exchange-correlation potential. Also compared are our structural results with the theoretical and experimental results presented by Ricinschi *et al.* (Ref. 4). The atomic geometry is expressed in lattice coordinates.

| | This work (LSDA) | | | This work ($\sigma$GGA) | | | Theory[a] | | | Expt.[a] |
|---|---|---|---|---|---|---|---|---|---|---|
| $a$ (Å) | | 3.70 | | | 3.670 | | | 3.67 | | 3.72 |
| $c$ (Å) | | 4.55 | | | 4.639 | | | 4.64 | | 4.67 |
| $c/a$ | | 1.230 | | | 1.264 | | | 1.264 | | 1.255 |
| Volume (Å$^3$) | | 62.252 | | | 62.478 | | | | | |
| Bi | 0.0 | 0.0 | 0.0000 | 0.0 | 0.0 | 0.0000 | 0.0 | 0.0 | 0.0000 | |
| Fe | 0.5 | 0.5 | 0.4567 | 0.5 | 0.5 | 0.4525 | 0.5 | 0.5 | 0.4390 | |
| O | 0.5 | 0.5 | −0.1327 | 0.5 | 0.5 | −0.1559 | 0.5 | 0.5 | −0.1640 | |
| | 0.5 | 0.0 | 0.3636 | 0.5 | 0.0 | 0.3037 | 0.5 | 0.0 | 0.3080 | |
| | 0.0 | 0.5 | 0.3636 | 0.0 | 0.5 | 0.3037 | 0.0 | 0.5 | 0.3080 | |
| Frequency of $B_1$ mode (cm$^{-1}$) | | 276.4 | | | 310.0 | | | | | |
| Fe magnetic moment ($\mu_B$) | | 4.94 | | | 4.90 | | | | | |

[a]Reference 4.

tively, of the sample grown by Ricinschi *et al.*[4] with the 5 Hz laser deposition scheme, and *structure IV* as the sample grown by Ricinschi *et al.*[4] with the 15 Hz laser deposition scheme. In our theoretical investigations, we first carried out total-energy calculations, within the *P*4*mm* symmetry, of all the four structures. The results after relaxing the atomic coordinates within the $\sigma$GGA scheme are presented in Table I. An analysis of the total-energy results indicates that the stability of the tetragonal structure is favored to some extent by a larger value of the in-plane lattice constant $a$ (i.e., closer to the substrate lattice constant of 3.89 Å) and to great extent by a larger value of the lattice-constants ratio $c/a$. We find that structures I and III are the least energetically favorable and are almost energetically degenerate. Structure II is energetically the most stable,[17] but Ricinschi *et al.* claim it to not to be a single-crystal phase but coexisting with structure III. The total energy of structure IV is at least as energetically stable as a structure comprised of equal percentage of coex-

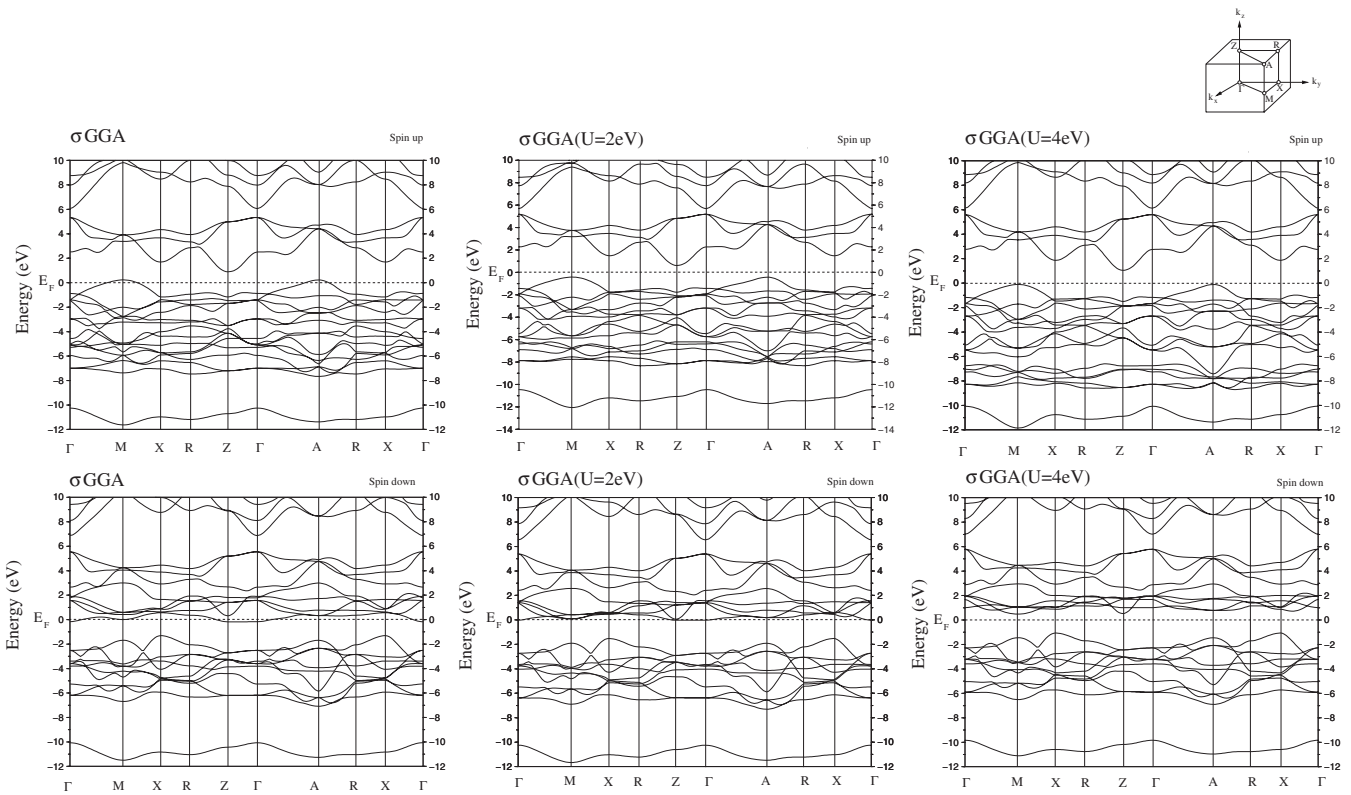


FIG. 1. Electronic band-structure results for tetragonal $BiFeO_3$ calculated within the $\sigma$GGA and $\sigma$GG+$U$ schemes.

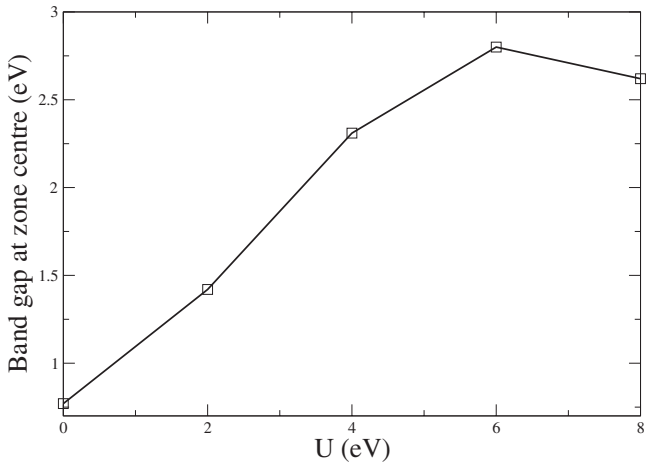


FIG. 2. Variation in the zone-center band gap (structure IV) with the $U$ parameter.

istence of structures II and III. In other words, we will consider structure IV to be the energetically most stable single-crystal phase for tetragonal BFO. Henceforth in the paper we will call structure IV as "the tetragonal structure." We have also carried out limited amount of investigations for all but structure IV. As shown in Table II, the equilibrium cell parameters and the atomic coordinates for structure IV agree very well with the experimental (using x-ray diffraction scans) results presented by Ricinschi *et al.*[4] Our results also agree with the *ab initio* theoretical results obtained by Ricinschi *et al.*—the small differences of results between the two sets of calculations are expected as we have applied the $\sigma$GGA scheme and Ricinschi *et al.* applied the LDA.

The interatomic distances and interlayer separations for the tetragonal structure (structure IV) are quite different from their corresponding values for the rhombohedral structure determined by us using the same computational method.[9] The Bi-O interplanar distances are 0.72 and 1.41 Å along [001] (or the $c$ axis) for the tetragonal structure and 2.31 and

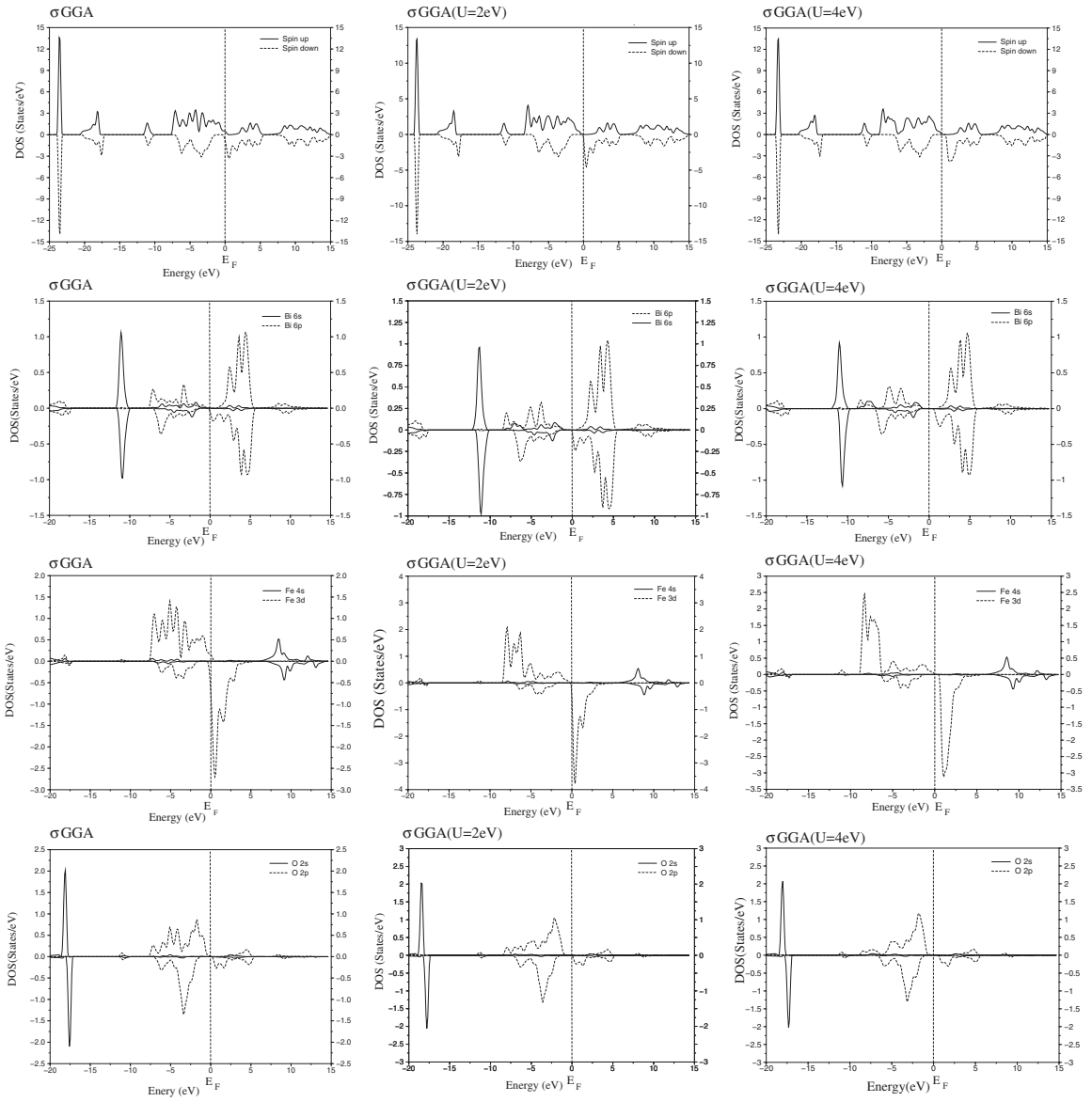


FIG. 3. Atomic projection of electronic PDOS for tetragonal $BiFeO_3$ calculated within the $\sigma$GGA scheme.

2.43 Å along [111] for the rhombohedral structure. Similarly, the Fe-O interplanar distances are 0.69 and 2.82 Å along [001] (or the $c$ axis) for the tetragonal structure and 1.92 and 2.10 Å along [111] for the rhombohedral structure. The shortest interatomic bond lengths are much shorter in the tetragonal structure: $d$(Fe-O)=1.96(2.50) Å and $d$(Bi-O)=2.31(2.56) Å for tetragonal (rhombohedral) structure. The O-Fe-O angle of 139° for the tetragonal phase is significantly smaller than 153° for the rhombohedral structure.

With the presently computed cell sizes and atomic coordinates and within the $\sigma$GGA scheme, the tetragonal phase (structure IV) is found to be 0.43 eV per BFO structural unit less stable than the rhombohedral phase,[9] confirming that the tetragonal phase is a metastable phase. Similar conclusion regarding the relative stabilities of the tetragonal and rhombohedral phases were obtained by Wang *et al.*[1] who used the local spin-density approximation (LSDA) scheme and by Ricinschi *et al.*[4] who used the LDA scheme. From our calculations within the $\sigma$GGA scheme, the magnetic moment of the Fe atom in the tetragonal phase is $4.90\mu_B$. This is larger than the $\sigma$GGA value of $3.87\mu_B$ obtained previously[9] for the rhombohedral phase. Within the $\sigma$GGA+$U$ scheme the magnetic moment for tetragonal BFO increases to $5.0\mu_B$: a value close to the bulk Fe magnetic moment.

It is useful to discuss differences in results obtained from the applications of LSDA vs $\sigma$GGA schemes. For this purpose we considered structure IV. We first obtained the equilibrium lattice parameters $a$ and $c$ and the relaxed atomic positions by using the spin-polarized form of Perdew-Zunger exchange-correlation scheme for both generating the pseudopotentials (using the VANDERBILT code[12]) for Bi, Fe, and O and for solving the Kohn-Sham equations. The results in Table II show that there are reasonably appreciable differences in the atomic geometries. We will discuss the difference in the LSDA vs $\sigma$GGA results for the frequency of a particular vibrational mode (the $B_1$ mode) later in this article.

It is also useful to compare the atomic geometry and total-energy results for the four tetragonal structures with the corresponding values for the rhombohedral bulk structure. Such a comparison, using the $\sigma$GGA scheme, is provided in Table I. It is clear that the in-plane lattice constant for each of the four tetragonal structures is smaller than the rhombohedral lattice constant. Structure I is pseudomorphically grown on the STO substrate with almost the same values of the in-plane ($a$) and perpendicular ($c$) lattice constants. In contrast, structures II, III, and IV have experienced in-plane compressive strains of 3.45%, 6.40%, and 6.02%, respectively, with the lattice parameter along the $c$ axis providing some strain relief. The large $c/a$ ratio gained for structure IV makes a significant contribution to the stability of phonon modes, as will be discussed later on. It should also be mentioned that compared to the rhombohedral structure, the volume per BFO formula unit is increased by 2.8%, 9.8%, 1.8%, and 3.8% for tetragonal structures I, II, III, and IV, respectively. The internal parameters for the tetragonal structures are also different from the rhombohedral structure, for example, there is a shortening of interplanar distances and the O-Fe-O angle for the tetragonal structures, as discussed earlier. The overall effect of the changes in cell dimensions and atomic geometry within the unit cell is to render the tetragonal structures as metastable, as their total energies are higher than that of the rhombohedral bulk.

TABLE III. Zone-center phonon results for the four tetragonal structures for $BiFeO_3$. The symmetry representations $A_1$, $B_1$, and $E$ are indicated. The frequencies are in $cm^{-1}$.

| Structure I $\sigma$GGA | Structure II $\sigma$GGA | Structure III $\sigma$GGA | Structure IV $\sigma$GGA | Structure IV $\sigma$GGA+$U$ ($U$=2 eV) |
|---|---|---|---|---|
| 59 ($E$) | ~0($E$) | 63 ($E$) | 80 ($E$) | 91 ($E$) |
| 167 ($A_1$) | 195 ($E$) | 179 ($A_1$) | 199 ($E$) | 207 ($E$) |
| 258 ($E$) | 212 ($A_1$) | 256 ($E$) | 227 ($A_1$) | 237 ($A_1$) |
| 265 ($A_1$) | 308 ($B_1$) | 294 ($A_1$) | 310 ($B_1$) | 332 ($B_1$) |
| 282 ($B_1$) | 328 ($E$) | 294 ($B_1$) | 357 ($E$) | 357 ($E$) |
| 309 ($E$) | 359 ($A_1$) | 330 ($E$) | 394 ($A_1$) | 427 ($A_1$) |
| 554 ($E$) | 554 ($E$) | 565 ($A_1$) | 618 ($E$) | 612 ($E$) |
| 569 ($A_1$) | 644 ($A_1$) | 582 ($E$) | 662 ($A_1$) | 662 ($A_1$) |

### B. Electronic band structure

The present work suggests that the applications of both the LSDA and $\sigma$GGA schemes produce a zero band-gap situation for the tetragonal phase of BFO (viz. for structure IV discussed above). This is not a big surprise, since the failure of the LSDA and $\sigma$GGA schemes in predicting correct electronic band structure near Fermi level for transition-metal oxides is well documented. For example, within the LSDA scheme, qualitatively wrong metallic ground state has been predicted.[15,18] Application of the LSDA+$U$ scheme is found to produce results which are both qualitatively and quantitatively correct. For FeO a choice of $U$=4.3 eV has been found to produce the observed insulating behavior.[15] With this in mind, we examined the band structure of tetragonal BFO with $U$=2 and 4 eV within the $\sigma$GGA+$U$ scheme. Figure 1 shows the spin-polarized band-structure results with

TABLE IV. Comparison of theoretical and experimental results for zone-center phonon modes for structure I of tetragonal $BiFeO_3$. Three symmetry representations $A_1$, $B_1$, and $E$ are indicated. The frequencies are in $cm^{-1}$.

| Present work ($\sigma$GGA) | Theory[a] | Expt.[a] |
|---|---|---|
| 59 ($E$) | 125.6 ($E$) | |
| 167 ($A_1$) | 129.8 ($A_1$) | 136 ($A_1$) |
| | 155.7 ($A_1$) | 168 ($A_1$) |
| | 206.0 ($A_1$) | 212 ($A_1$) |
| 258 ($E$) | 245.4 ($E$) | 257 ($E$) |
| 265 ($A_1$) | | |
| 282 ($B_1$) | 332.6 ($B_1$) | |
| 309 ($E$) | 453.6 ($E$) | 464 ($E$) |
| 554 ($E$) | 530.8 ($E$) | 546 ($E$) |
| 569 ($A_1$) | | |

[a]Reference 3.

and without the consideration of the effective screened on-site interaction parameter $U$.

Figure 2 shows the variation in the band gap at the zone center as a function of the parameter $U$. This suggests that an optimum band-gap opening can be expected for the choice of $U$ between 4 and 6 eV. From this examination and considering the suggestion of 4.3 eV from previous research on FeO by Cococcioni and Gironcoli,[15] we believe that a choice close to 4 eV would be more appropriate. It should be made clear that in this work we are discussing the Kohn-Sham band gap within the $\sigma$GGA and $\sigma$GGA+$U$ schemes. Kohn-Sham band gaps cannot firmly be identified either with optical band gaps or with quasiparticle band gaps. However, in practice Kohn-Sham gaps are usually compared and identified with quasiparticle gaps. A clear distinction between the Kohn-Sham, quasiparticle, and optical gaps can be found in a recent review article by Kümmel and Kronik.[19]

A closer examination of the electronic bands for tetragonal BFO reveals that within the $\sigma$GGA scheme both spin-up and spin-down bands exhibit metallic behavior. For $U=2$ eV, near the Fermi level the spin-up band is slightly pushed down and the spin-down band is slightly pushed up. However, for this rather small choice of $U$ the spin-down channel still shows metallic behavior. The general behavior of the movement of spin-up and spin-down bands near the Fermi level becomes more pronounced for larger values of $U$, and a band gap opens. For $U=4$ eV we find a direct band gap of 0.55 eV at the $M$ point in the Brillouin zone, with the highest occupied and lowest unoccupied bands being spin-up and spin-down polarizations, respectively. The small and direct band-gap nature of the tetragonal phase is clearly very different from the larger and indirect band-gap nature of the rhombohedral phase (for the latter an indirect band gap of 1.8 eV was calculated within the $\sigma$GGA+$U$ with $U=4$ eV).[9]

In order to understand the origin of the band-gap opening with the parameter $U$, we have plotted the atomic-projected electronic density of states (PDOS) in Fig. 3. The top row shows the spin-polarized total density of states and the other rows indicate spin-polarized angular-momentum-dependent contributions from different atomic species. For the purpose of examining band-gap opening, we focus our examination of the features near the Fermi level $E_F$. The total DOS curves suggest that the contributions are larger from the spin-up (down) states below (above) the Fermi level $E_F$. In the immediate vicinity of $E_F$, the contribution from the oxygen atoms is almost negligible, the contribution from Bi $6p$ states is approximately one tenth of the total value, and the dominant contribution is from the Fe $3d$ states. The on-site interaction parameter $U$ within the $\sigma$GGA+$U$ scheme generally pushes the peak on the lower side of $E_F$ to a lower energy and the peak on the higher side of $E_F$ to a higher energy, thus helping to open a finite band gap. However, very little change is noticed with $U=2$ eV, suggesting that this value of the on-site interaction coefficient is virtually ineffective. With $U=4$ eV, occupied as well as unoccupied peaks belonging to both Bi $5p$ and Fe $3d$ orbitals have moved away from the Fermi level.

### C. Phonon-dispersion relations

We will discuss the results of our *ab initio* phonon calculations for the tetragonal structure of BFO in two parts. We

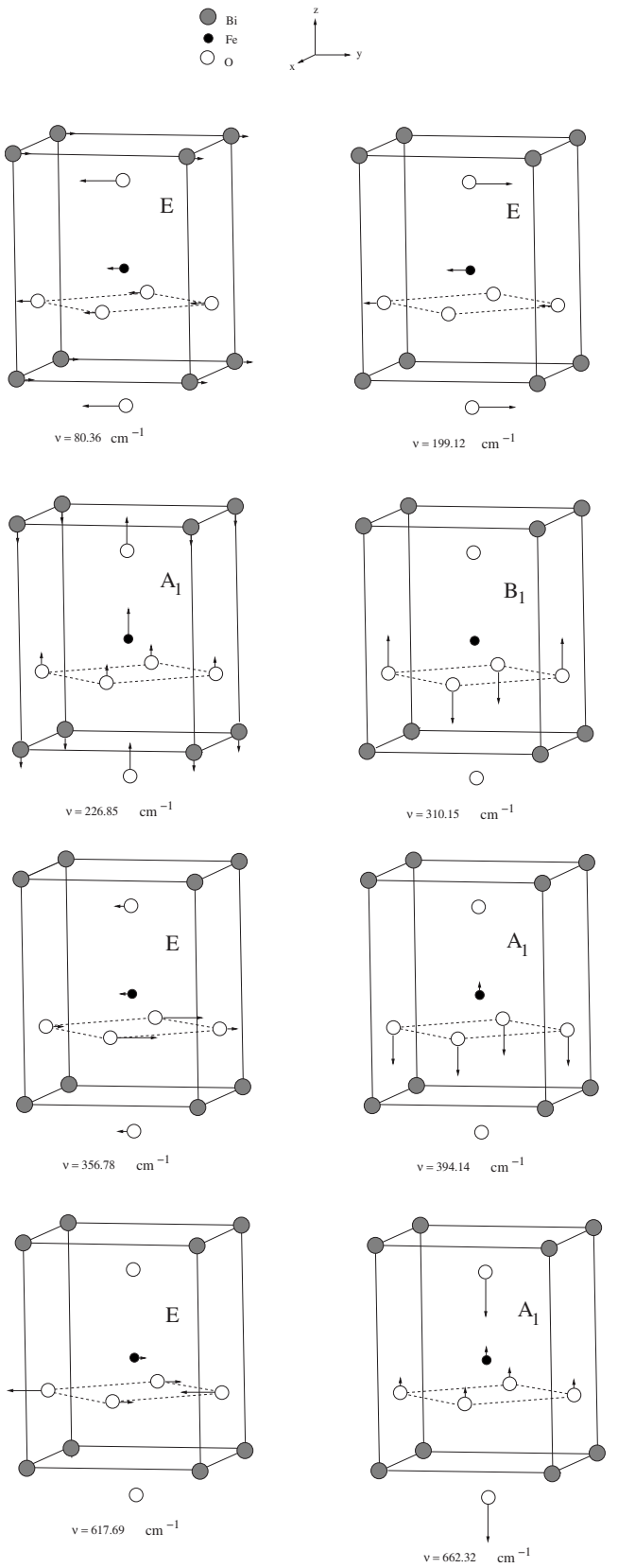


FIG. 4. Atomic displacement patterns for zone-center Raman-active phonon modes in tetragonal $BiFeO_3$ calculated within the $\sigma$GGA scheme. The solid lines show the unit cell, and the dotted lines indicate the plane containing equatorial oxygen atoms within the unit cell.

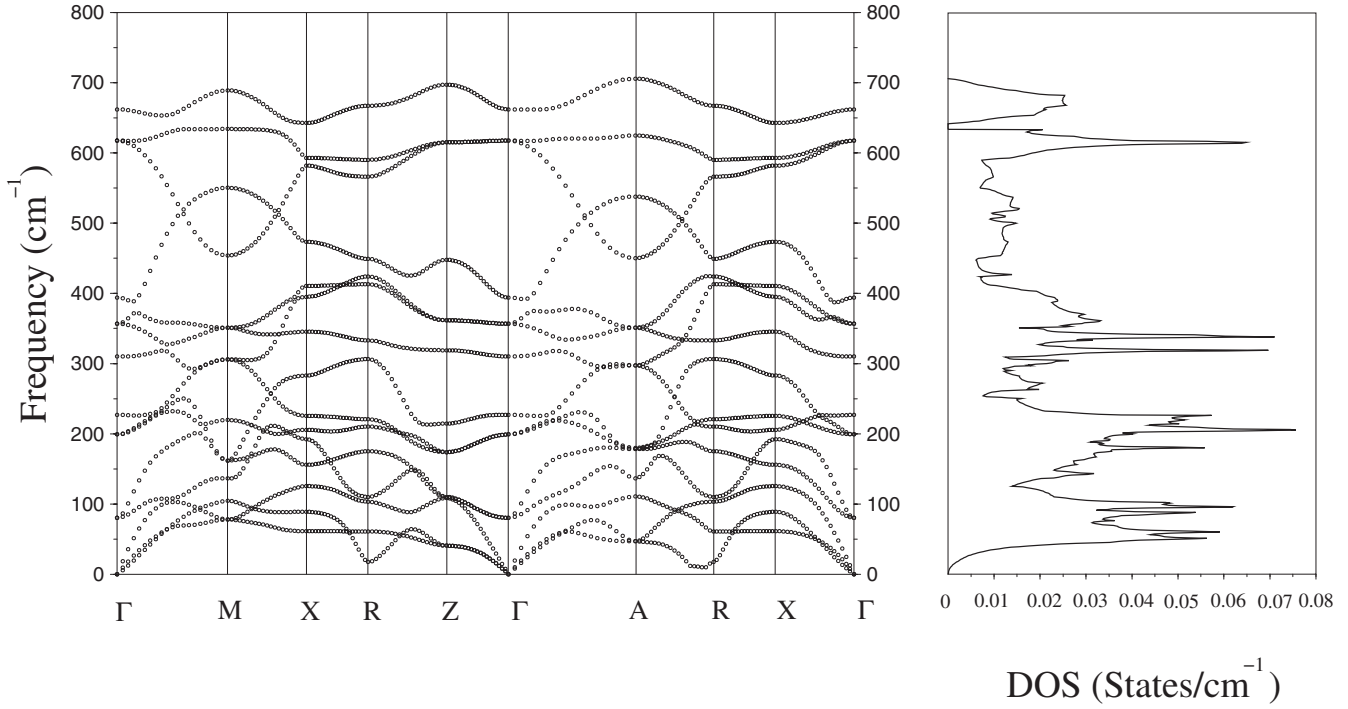


FIG. 5. Phonon-dispersion relation and vibrational density of states in tetragonal $BiFeO_3$ calculated within the $\sigma$GGA scheme.

will first describe the energy location and polarization characteristics of the zone-center phonon modes. These results will be compared and contrasted with available polarized Raman-scattering measurements. A brief comparison of the results with the rhombohedral structure will also be made. In addition to discussing results at the zone center, we will present phonon-dispersion curves along various symmetry directions and identify important features in the vibrational density of states.

### *1. Zone-center modes*

Within the tetragonal symmetry with the point-group $4mm$ ($C_{4v}$) and space group $P4mm$ ($C_{4v}^1$), zone-center phonon modes for BFO can be expressed with the representation $\Gamma=4A_1+B_1+5E$, where $A_1$ and $B_1$ are one-dimensional irreducible representations and $E$ is a two-dimensional irreducible representation. A total of 15 modes arise from the five atoms within a unit cell. Three of these include the longitudinal-acoustic mode and the transverse-acoustic modes, with representations $A_1$ and $E$, respectively. The 12 optical modes are all Raman active and can be expressed with the representation $\Gamma_R=3A_1+B_1+4E$. In Table III we have presented the energy locations and the irreducible representations of the 12 optical modes for all the four structures calculated presently within the $\sigma$GGA scheme. Table IV presents a comparison of our results for structure IV with (i) polarized Raman measurements and (ii) a short-range force-constant lattice dynamics model both by Singh *et al.*[3]

The results presented in Table III reveal that both the location (frequency) and symmetry ordering of the zone-center vibrational modes change significantly between the four tetragonal structures considered in this work. For example, the symmetry of the highest mode is $A_1$ for structures I, II, and IV, whereas it is $E$ for structure III. There is a spread of approximately 15% in the frequency values obtained for the four structures for the highest mode. There is also a spread of approximately 15% in the frequency of the $B_1$ mode, which arises from the vibration of the equatorial oxygen atoms against each other along the $c$ axis. A significant feature of structure II is that the lowest optical modes of the $E$ symmetry have dipped down to a frequency close to zero. This may be taken as an indication that structure II characterized with the shortest in-plane lattice constant $a$ among the four phases is unstable.

It is also useful to discuss the role of $\sigma$GGA over the LSDA in phonon calculations. For this purpose we examine the difference in the results for the $B_1$ mode for structure IV with the choice of LSDA vs $\sigma$GGA. To do this, we first obtained the equilibrium lattice parameters $a$ and $c$ and the relaxed atomic positions, by using the spin-polarized form of Perdew-Zunger exchange-correlation scheme for both generating the pseudopotentials (using the VANDERBILT code[12]) for Bi, Fe, and O and for solving the Kohn-Sham equations. The results in Table II show that there are reasonably appreciable differences in the atomic geometries. More noticeable is the difference in the frequency of the $B_1$ mode presented in Table II. The LSDA scheme produces a lower value of the $c$ lattice parameter (with $c/a=1.230$). Consistent with the discussion presented before, the smaller $c/a$ ratio results in a reduction of 11% for the $B_1$ mode frequency from the application of LSDA compared to $\sigma$GGA. However, there is no appreciable difference in the Fe magnetic moment with the choice of LSDA vs $\sigma$GGA.

There is some change in phonon frequencies when the $U$ parameter is included within the $\sigma$GGA+$U$ scheme. However, such changes are rather small and there is no systematic "shift" in mode frequencies when the $U$ parameter is in-

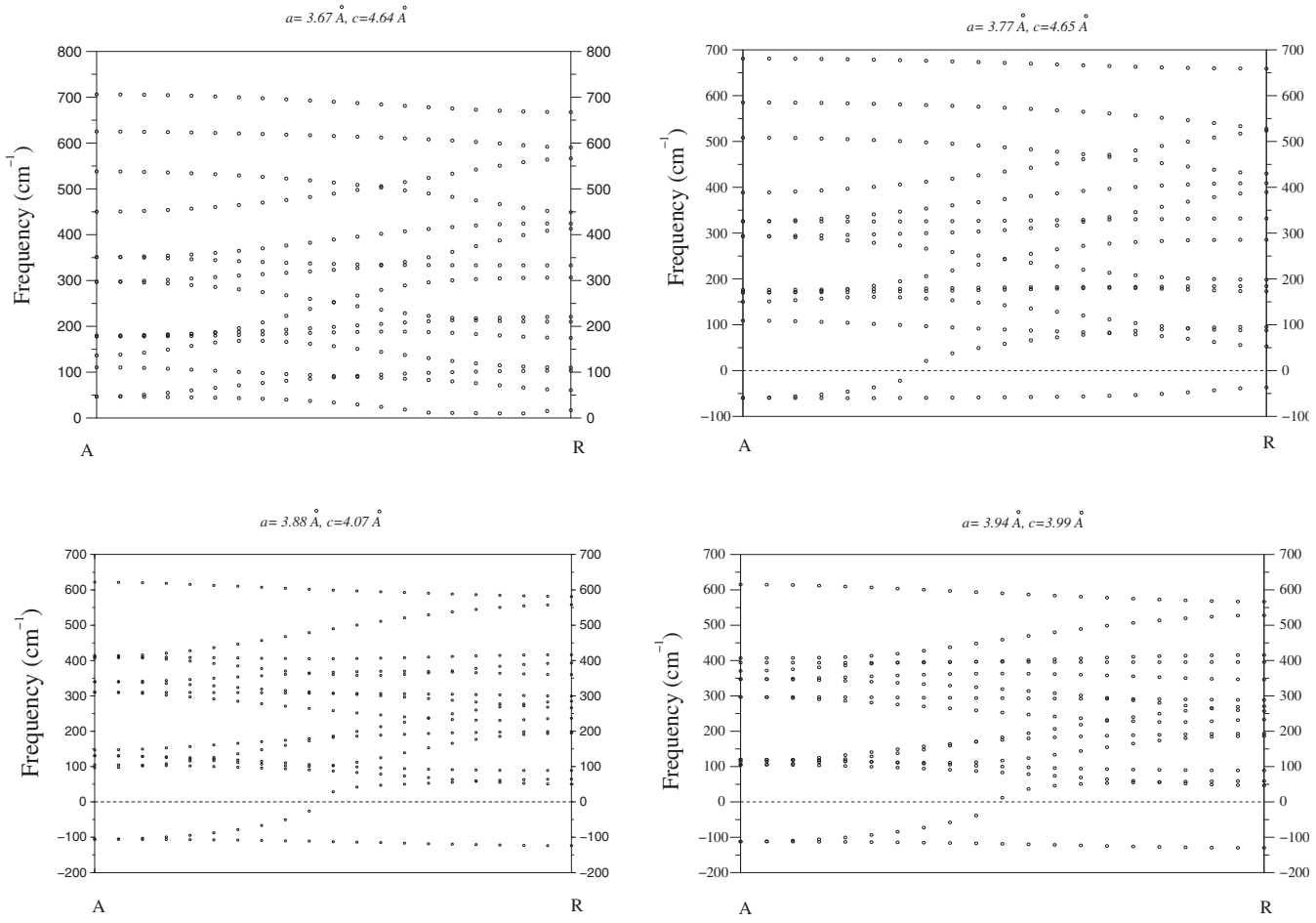


FIG. 6. Phonon-dispersion curves (from $\sigma$GGA calculations) along the $A$-$R$ direction for all four tetragonal structures studied in this work. Imaginary frequency values are presented along the negative $y$ axis.

cluded. This can be appreciated from the results presented for structure IV in Table III, with $U=2$ eV. This table shows that while some modes are totally unaffected, the frequency of others changes by no more than 14%. We further find that there is no appreciable change in the results by increasing $U$ to 4 and 6 eV.

In Table IV we have compared our results of the zone frequency phonon modes for structure I with the theoretical and experimental results presented by Singh *et al.*[3] From their Raman measurements, Singh *et al.* observed three $A_1$ and three $E$ modes. From the application of a simple lattice dynamical model, on the other hand, they obtained three $A_1$, one $B_1$, and four $E$ modes. Our theoretical results agree with their theoretical results for the number of modes of the $A_1$, $E$, and $B_1$ symmetries. However, only a few modes seem to agree between our work and the experimental and theoretical results presented by Singh *et al.* It is interesting to note that there is good match for the $B_1$ frequency obtained from the two theoretical works. This can be expected, as this mode arising from the short-range interaction between the two equatorial oxygen atoms in the (shown in Fig. 4) can be fairly well determined from the simple short-range force-constant scheme employed by Singh *et al.* Below the $B_1$ mode, there is good match for one of the $A_1$ modes and also for one of the $E$ modes. Above the $B_1$ mode, there is also good match for one of the $E$ modes. However, there are noticeable discrepancies. In particular, our work suggests that the highest mode is of the $A_1$ symmetry, while both the theoretical and experimental works by Singh *et al.* reported it to be of the $E$ symmetry. We believe that another attempt on polarized Raman measurements should be made to resolve these discrepancies.

It is also useful to present a comparison of the phonon results for the most stable of the tetragonal phase (structure IV) and the rhombohedral phase of BFO. From our works (present and in Ref. 9) it is found that the highest phonon mode in the tetragonal phase ($P4mm$) has frequency $\sim$662 cm$^{-1}$ of $A_1$ representation and of frequency $\sim$590 cm$^{-1}$ of $A_2$ representation in the rhombohedral phase ($R3c$). There is some similarity between the vibrational pattern, as well as energy location, of the $B_1$ mode in tetragonal BFO and one of the $A_1$ modes in rhombohedral BFO. Both these modes arise due to out-of-phase vibrations of basis atoms in the oxygen plane within the unit cell (normal to [001] for tetragonal BFO and normal to [111] for rhombohedral BFO) and lie at approximately the same frequency.

### *2. Dispersion curves and density of states*

In Fig. 5 we have presented the full phonon-dispersion curves for structure IV along the various symmetry direc-

tions within the irreducible part of the tetragonal Brillouin zone. Also presented in that diagram is the vibrational density of states. A few observations can be made. One of the transverse-acoustic branches shows a dip in its dispersion curve near the *R* symmetry point. This indicates that it is a soft branch for structure IV. The lower transverse-acoustic branch shows a flat dispersion behavior at almost all zone-edge points and along several symmetry directions. Several other branches also show flat dispersion behavior along several symmetry directions. The flat dispersion curves have produced several sharply defined Van Hove singularities in the density of states curve. The highest branch of the $A_1$ symmetry at the zone center is split from the continuum of the rest of the branches, thus creating a small gap in the density of states at around 650 $cm^{-1}$.

Away from the zone center, the degenerate *E* modes split. Our work shows that the lower-split branch from the highest zone-center *E* mode and the upper-split branch of the second-highest zone-center *E* mode are the most dispersive and cross each other along the symmetry directions Γ-*M*, *M*-*X*, Γ-*A*, and *A*-*R*. These behaviors can be appreciated by noting from Fig. 4 that these branches mainly originate from vibrations of the oxygen atoms in the equatorial plane. For finite in-plane phonon vectors, such as along Γ-*M*, a linear combination of in-phase and out-of-phase atomic vibrations of the two equatorial oxygen atoms can be formed.

The observation of a soft branch for structure IV along the *A*-*R* symmetry direction signals similar behavior of one or more phonon branches for other tetragonal structures for BFO. To investigate this, we have plotted in Fig. 6 the dispersion curves along *A*-*R* for the other three structures considered in this work. Unstable phonon modes are found to develop all along the *A*-*R* direction for structures I, II, and III. Whereas structures I and III are characterized with low $c/a$ values, structure II is characterized with a reasonably large $c/a$ ratio but with a much smaller *a* lattice constant. We also examined the effect of smaller values of the in-plane lattice constant *a* and the ratio $c/a$. A change of 2.5% in these values results in the development of unstable modes (i.e., imaginary frequencies) around the *A* and *M* points. These phonon test results indicate that stable tetragonal structures for BFO require deposition schemes that result in in-plane lattice constant *a* close to the lattice constant of STO and a larger value of *c*.

## IV. SUMMARY

We have reported results of *ab initio* calculations for the stability, electronic structure, and lattice dynamical properties of the four tetragonal structures of $BiFeO_3$ that have been presented in the literature. From these studies we have concluded that the most stable of these structures is the single-phase sample prepared by Ricinschi *et al.*[4] deposited with a 15 Hz laser frequency using the STO(001) substrate. This structure (structure IV) is characterized by an in-plane lattice constant *a* which is 6% smaller than the STO lattice constant but with a large $c/a$ ratio of 1.264. This system is predicted to be semiconducting with a direct Kohn-Sham band gap of approximately 0.55 eV, much smaller than the (indirect) Kohn-Sham band gap for the rhombohedral phase. The magnetic moment per Fe atom (within the σGGA scheme) in the tetragonal phase of $4.90\mu_B$ is larger than $4.25\mu_B$ in the rhombohedral phase.

A detailed study of the phonon-dispersion relations suggests that three of the four tetragonal structures are characterized by the presence of unstable phonon branches along the *A*-*R* symmetry direction. Our results of zone-center phonon modes for one of the structures (for the low-laser-frequency-deposited tetragonal structure) have been compared with the polarized Raman measurements and a simple theoretical model by Singh *et al.*[3] and significant differences have been noted. A detailed description of the phonon-dispersion relations for the most stable single-phase structure (structure IV) has been presented. It is found that the highest optical phonon branch is split from the continuum of the rest of the branches by a small gap. The highest phonon mode with frequency ~662 $cm^{-1}$ of $A_1$ representation in the tetragonal phase ($P4mm$) can be readily distinguished from the frequency ~590 $cm^{-1}$ of $A_2$ representation in the rhombohedral phase ($R3c$).

## ACKNOWLEDGMENTS

This work was carried out with the support of EPSRC (U.K.) through Grant No. EP/E019528/1. We thank Manoj Singh for getting us interested in this problem, and for discussion of the phonon results at the initial stages of the project.

*Permanent address: Sakarya Üniversitesi, Fen-Edebiyat Fakültesi, Fizik Bölümü, 54187, Adapazarı,Turkey.

[1] J. Wang, J. B. Neaton, H. Zheng, V. Nagarajan, S. B. Ogale, B. Liu, D. Viehland, V. Vaithyanathan, D. G. Schlom, U. V. Waghmare, N. A. Spaldin, K. M. Rabe, M. Wuttig, and R. Ramesh, Science **299**, 1719 (2003).

[2] M. K. Singh, H. M. Jang, S. Ryu, and M.-H. Jo, Appl. Phys. Lett. **88**, 042907 (2006).

[3] M. K. Singh, S. Ryu, and H. M. Jang, Phys. Rev. B **72**, 132101 (2005).

[4] D. Ricinschi, K.-Y. Yun, and M. Okuyama, J. Phys.: Condens. Matter **18**, L97 (2006).

[5] H. Fukumura, H. Harima, K. Kisoda, M. Tamada, Y. Noguchi, and M. Miyayama, J. Magn. Magn. Mater. **310**, e367 (2007).

[6] M. Cazayous, D. Malka, D. Lebeugle, and D. Colson, Appl. Phys. Lett. **91**, 071910 (2007).

[7] S. Kamba, D. Nuzhnyy, M. Savinov, J. Šebek, J. Petzelt, J. Prokleška, R. Haumont, and J. Kreisel, Phys. Rev. B **75**, 024403 (2007).

[8] P. Hermet, M. Goffinet, J. Kreisel, and Ph. Ghosez, Phys. Rev. B **75**, 220102(R) (2007).

[9] H. M. Tütüncü and G. P. Srivastava, J. Appl. Phys. **103**, 083712

(2008).
[10] S. Baroni, S. de Gironcoli, A. Dal Corso, and P. Giannozzi, Rev. Mod. Phys. **73**, 515 (2001).
[11] http://www.pwscf.org
[12] D. Vanderbilt, Phys. Rev. B **41**, 7892 (1990).
[13] R. O. Jones and O. Gunnarsson, Rev. Mod. Phys. **61**, 689 (1989).
[14] J. P. Perdew, K. Burke, and M. Ernzerhof, Phys. Rev. Lett. **77**, 3865 (1996).
[15] M. Cococcioni and S. de Gironcoli, Phys. Rev. B **71**, 035105 (2005).
[16] H. J. Monkhorst and J. D. Pack, Phys. Rev. B **13**, 5188 (1976).
[17] From an extensive set of total-energy calculations we find that the lowest total energy corresponds to a structure with the cell parameters $a=3.78$ Å and $c/a=1.31$. The total energy of this structure is 0.27 eV/cell lower than that of structure II. However, for the equilibrium atomic geometry with these cell parameters, we have obtained unstable phonon modes along several symmetry directions. This geometry, therefore, has not been discussed in the text.
[18] W. E. Pickett, S. C. Erwin, and E. C. Ethridge, Phys. Rev. B **58**, 1201 (1998).
[19] S. Kümmel and L. Kronik, Rev. Mod. Phys. **80**, 3 (2008).